Synthesis, simulation & spectroscopy: physical chemistry of nanocrystals

J. F. Suyver

Debye Institute, Physics and Chemistry of Condensed Matter, Utrecht University, P.O. Box 80.000, 3508 TA Utrecht, The Netherlands.
E-mail: j.f.suyver@phys.uu.nl

Abstract

Experiments on nanocrystalline semiconductors form a wide and rapidly expanding field of research. This chapter concentrates on two very different topics within this field. In the first part, pair formation of dopant ions in nanocrystals is discussed. After a general introduction on the influence of pair formation on the luminescence properties, pair formation in nanocrystals is discussed. Due to a difference between the connectivity for sites in the bulk and at the surface, the fraction of dopant pairs depends on the crystallite size. Simulations of the statistical distribution of dopant pair states in a nanocrystal as a function of crystal structure, size and dopant concentration are presented. A closed form approximation for the results of the simulations is derived and the validity is tested. The work presented can be used to estimate dopant pair concentrations in the case of random substitution or a lower limit for the pair concentration if preferential pair formation occurs.

The second part of the chapter discusses the luminescence of a single nanocrystalline semiconductor particle. The absence of inhomogeneous broadening and other ensemble averaging effects has provided exciting new insight into the luminescence and quenching mechanisms. The linewidth, blue shift and bleaching of the luminescence of single CdSe/ZnS core/shell nanocrystals are shown and discussed. Finally, potential applications of nanocrystals as luminescent labels in biological systems are presented and a few challenges for future research are discussed.

1 Introduction

Materials with nanometer dimensions are currently under extensive study throughout the world [1–5]. A wide variety of physical and chemical methods and experiments make it possible to study nanometer-sized structures in ever greater detail. Research in this area is driven not just by scientific curiosity, as new applications based on nanosized building blocks are expected [6, 7]. In computer chips, where with (V)UV lithography patterns of $\sim$100 nm are routinely made, the 'hunger' for smaller sized structures is very clear. Even smaller structures (typically $\sim$20

nm) will be needed to realize the higher speeds and information storage capacities of the computers of the future. Knowledge of the interesting changes in the electronic structure as the particles become smaller will also be essential for future applications. Established synthesis procedures to make very small ($1-10$ nm) nanocrystals (NCs) allow for fundamental research on the changing properties as a function of particle size, and this has resulted in fascinating discoveries [1–3, 7, 8]. In electroluminescent devices (in which electrical current is converted into visible light) much smaller dimensions could be obtained by generating luminescence from nanocrystals or from luminescent ions inside the nanocrystals [5, 6].

"*Systems with spatially confined structures*" represents a very broad field, and therefore only two (quite different) topics within this theme will be discussed in this chapter. Light-emitting nanocrystals[1] in future applications could very well have a dopant ion as the light-emitting species. It is for this reason that the first part of this chapter will deal with the calculation of dopant pair states in a nanocrystal. Effects of pair formation of dopants on the luminescence of bulk crystals is discussed first, followed by simulation and theory developed for pair formation in nanocrystals. For the second part of this chapter, the luminescence spectroscopy of single nanocrystals is reviewed, some characteristic experiments are discussed and a few selected challenges for future research are also presented.

2 Dopant pair-state calculations

The formation of pairs of dopant-ions can be important for the magnetic and optical properties of materials [9, 10]. For example, the luminescence lifetime of the Mn^{2+} emission in ZnS:Mn^{2+} decreases and the emission shifts to longer wavelengths when Mn^{2+} pairs are formed. This is due to relaxation of the spin selection rule for the optical transition through the magnetic interaction between the ions [11–14]. In oxide nanocrystals (e.g. YVO_4 and Y_2O_3) the luminescence properties of rare earth ions like Ce^{3+}, Sm^{3+}, Eu^{3+}, Tb^{3+} and Dy^{3+} have been studied in detail [15–17]. Also here, the luminescence properties are significantly influenced by dopant pair formation. For example, the emission from higher ^5D_J levels of Eu^{3+} or Tb^{3+} is quenched by cross-relaxation processes in pairs, whereas this is not observed for single ions [18].

2.1 Pair-states in a bulk crystal

Before the discussion of a nanocrystal is presented, it is useful to be reminded of some of the effects that high dopant concentrations have on the luminescent

[1] Also known as: 0D-structures, quantum dots, artificial atoms, Q-dots, (nano)clusters, ... In order to avoid confusion, the remainder of this chapter will only discuss *nanocrystals*.

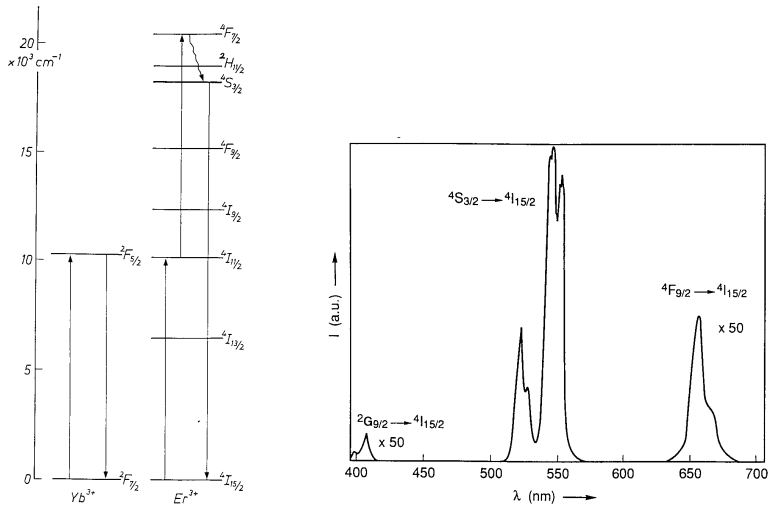

Figure 1: (Left) Energy level diagram and (right) photoluminescene spectrum of Er^{3+} and Yb^{3+} doped ZBLAN glass. Excitation wavelength was at 970 nm. Measured at 300 K. Data taken from Ref. [20] with kind permission from the authors.

properties of a bulk crystal. Many interesting effects and changes in luminescence properties have been observed for pairs and clusters of dopant ions.

In a crystal where Yb^{3+} and Tb^{3+} ions are located close together, cooperative energy transfer can take place [19]. By the cooperative energy transfer process, infrared radiation (absorbed by the Yb^{3+} ions) is converted into visible light (the green $^5D_4$ emission from the Tb^{3+} ion). In such a process, for example, two excited Yb^{3+} ions (in the $^2F_{5/2}$ state) simultaneously transfer their energy to the Tb^{3+} ion (in the $^7F_6$ ground state), exciting it into the $^5D_4$ level. In this example, the final state of the donor ions (Yb^{3+}) is the ground state, but this need not be the case. Furthermore, it is not necessary that the transition on the two donor ions is the same. Other cooperative energy transfer processes in pairs and clusters of luminescent ions have also been observed, for example with Pr^{3+} [19].

A second type of energy transfer, is the Auzel-process, or upconversion [19]. In this process, two step resonant energy transfer occurs and infrared radiation can be very efficiently converted into visible light. An example of this process is found in Er^{3+} and Yb^{3+} doped glass. The energy level diagram and a typical luminescence spectrum are shown in figure 1. In this case, two Yb^{3+} sequentially transfer their energy to the same Er^{3+} ion. The $^2F_{7/2} \rightarrow {}^2F_{5/2}$ transition on the Yb^{3+} ion has a larger optical excitation cross-section than the $^4I_{15/2} \rightarrow {}^4I_{11/2}$ transition on the Er^{3+} ion. Therefore, with an excitation wavelength of 970 nm,

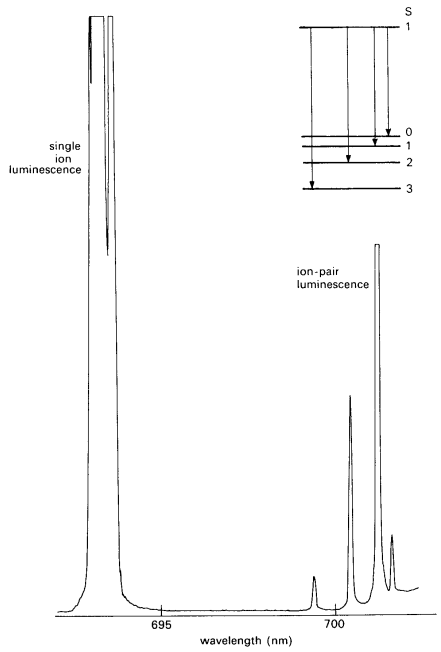

Figure 2: Photoluminescene spectrum of Cr^{3+} doped Al_2O_3 (ruby). Excitation wavelength was 400 nm. Measured at 2 K.

most of the excited ions will be Yb^{3+} ions. The first Yb^{3+} ion brings the Er^{3+} ion into the (long lived) $^4I_{11/2}$ state by energy transfer and the second one excites the Er^{3+} ion further into the $^4F_{7/2}$ state, from which it decays nonradiatively to the $^4S_{3/2}$ state. The visible luminescence from this state to the ground state ($^4S_{3/2}$ $\rightarrow$ $^4I_{15/2}$) can be quite intense and total luminescence energy efficiencies for the upconversion emission of more than 20% have been observed [20].

A completely different effect of pair formation can be observed in the luminescence spectra of Cr^{3+} doped Al_2O_3 (ruby), as is shown in figure 2. The sharp lines at 694 nm, typical for a ruby laser, are due to emission from isolated Cr^{3+} ions. The transition involved is the spin forbidden $^2E \rightarrow {}^4A_2$ transition within the d^3 configuration of the Cr^{3+} ion. However, when more Cr^{3+} is incorporated into the Al_2O_3 lattice, four additional lines (at $699 - 704$ nm) arise in the luminescence spectrum. These lines are due to emission from pairs of exchange-coupled Cr^{3+} ions.

An exchange interaction occurs between two ions when their electron clouds overlap[2]. When all constant terms are neglected, the exchange interaction between

[2]This interaction can also take place when the electron clouds do not directly overlap. In this

ions A and B can be written as

$$-\sum_{i,j} J_{A(i),B(j)} \mathbf{s}_{A(i)} \cdot \mathbf{s}_{B(j)} \ , \tag{1}$$

where the summation over i, j represents a summation over all the electrons of ions A and B, respectively. The coupling-parameter $J_{A(i),B(j)}$ is related to the strength of the Coulomb interaction between two electrons (electron i on ion A and electron j on ion B).

Exchange interaction between neighbouring Cr^{3+} ions gives a modified energy level scheme in which the total magnetic (spin) moment J for both ions in the $^4A_2$ ground state varies from 0 to 3. For one ion of the pair in the ^2E excited state J is 1 or 2. In figure 2 the situation is depicted in the top right corner of the emission spectrum. The theoretically calculated separation between the different J states in the ground state is J, $2J$ and $3J$ [19]. This splitting is nicely reproduced in the emission spectrum. Also note that the strongest emission line of the ion pair at 702 nm corresponds to the $J = 1$ to $J = 1$ transition. For this transition the spin-selection rule is relaxed. The relaxation of the spin-selection rule is also evident from the change in lifetime. For the isolated Cr^{3+} ions the lifetime of the spin- and parity-forbidden $^2E \rightarrow {}^4A_2$ emission is 3.5 ms. For the Cr^{3+} pair emission shown in figure 2, the lifetime is 0.8 ms. Both lifetimes reported were measured at room temperature [21].

In all these examples the pair-state emission is markedly different from the single-ion luminescence. Already in 1958 Behringer was able to calculate the number of single-ions and pair-ions that one expects for a certain percentage of dopants introduced in the lattice [22]. These numbers have been compared with experimental results obtained from luminescence measurements (on Gd^{3+} doped Lu_2O_3 and other rare-earth compounds [23]) and good agreement has been found. Naturally, when preferential pair-formation plays a role, the values obtained by Behringer represent a lower limit.

2.2 Differences in a nanocrystal

In a normal (infinite) crystal, the surface does not influence the statistics for pair formation. This will not be the case in a nanocrystal. Because the number of nearest-neighbors is lower at the surface of the crystal than in the bulk, the fraction of dopant ion-pairs for a given dopant concentration in very small crystal will be size dependent.

A natural question to ask is whether the percentage of pair-states can be evaluated analytically for any given crystal with an arbitrary size and dopant-concentration.

case, the interaction is mediated through the intervening ions. This is called *superexchange*, which has a smaller interaction strength than for direct wavefunction overlap.

Unfortunately, the answer to this question is, in general, "No". This is due to the fact that not only the number of dopants is important, but also the *combinatorial possibilities* that these dopants can form in the nanocrystal. Even when two dopants do not form a pair-state (for example, when they are two nearest-neighbor distances apart), their relative positions influence the probability for pair formation with a third dopant (e.g. when it is located on any of the lattice positions that are only one nearest-neighbor distance from the two dopants already present in the lattice). The number of combinatorial possibilities diverges exponentially with the number of lattice positions, which makes it impossible to find a closed-form analytical solution to this problem. It is for these reasons that numerical simulations are needed in the case of a nanocrystal. It may be interesting for the reader to know that in an infinite crystal, even though the number of combinations is infinite, exact analytical solutions to this problem can be found. This is due to the fact that most combinatorial possibilities cancel, or become insignificant compared to the highest-frequency one.

2.3 Simulations and numerical results[3]

2.3.1 Definition of the algorithm

The lattice positions in any crystalline material are characterized by the crystal structure combined with the lattice parameter a [24]. By the introduction of the dimensionless parameter $\rho \equiv (r/a)$ a formalism is described that does not depend on a and holds for any crystal with the same crystal structure. The method presented here is generally applicable to every nanocrystalline system. In order to calculate values, a choice of the crystallographic structure is made. In the remainder of this section, the zincblende structure (space group $F\ \bar{4}\ 3m - T_d^2$) is chosen, as an example. This crystal structure is found in a range of semiconductors such as in CuBr, ZnS, CdSe, InP and GaAs, which are widely studied, also as nanocrystalline materials.

The number of lattice positions available, n in a spherical crystal of radius r, will depend on the cube of the radius via

$$n(r) \;=\; 4 \cdot \frac{4}{3}\pi \left(\frac{r}{a}\right)^3 \;=\; \frac{16\pi}{3}\rho^3 \;\equiv\; n(\rho)\;, \tag{2}$$

where the extra factor of 4 is determined by the number of lattice positions in the zincblende unit cell. Note that equation (2) is exact only if $\rho \gg 1$. Since this is not the case in the system under investigation, where ρ is typically between 2 and

[3]The remainder of this section is largely based on the paper "*Probabilities for dopant pair-state formation in a nanocrystal: simulations and theory*", by J. F. Suyver, R. Meester, J. J. Kelly and A. Meijerink, which has been submitted to Physical Review B (June 2001).

10, equation (2) should only be viewed as an approximation. The exact value of n is determined by analysis of the overlap of the zincblende crystal with a sphere of radius ρ centered at a lattice position. The influence of this procedure, and data regarding the number of lattice positions on the surface and in the bulk of the nanocrystal, are discussed in detail in section 2.4.1.

To describe correctly the nanocrystal, the complete lattice of the crystal is defined via the set of n vectors $\{\mathbf{p}_a\}$ that point to each of these lattice positions. The situation in which a fraction f of these lattice positions is filled with dopant ions, is simulated by choosing a random subset $\{\mathbf{q}_b\}$ of $k = fn$ different vectors from the complete set $\{\mathbf{p}_a\}$. A pair-state in this crystal configuration is now defined to occur if and only if

$$\exists \lambda > \sigma \in \mathbb{Z} : |\mathbf{q}_\lambda - \mathbf{q}_\sigma| = d_{\mathrm{NN}} \ , \tag{3}$$

where d_{NN} represents the nearest-neighbor distance. For the zincblende crystal structure, $d_{\mathrm{NN}} = a/\sqrt{2}$.

By choosing the random subset $\{\mathbf{q}_b\} \subset \{\mathbf{p}_a\}$ a very large number of times, one approximates the actual probabilities for pair-state formation. Let $\Phi(n,k)$ and $\Psi(n,k)$ represent the probability for at least one pair-state, and the percentage of positions that are part of a pair-state (relative to the number of dopants present in the nanocrystal) respectively.

To find the probability for the presence of at least one pair-state in the nanocrystal, a set of $1 \cdot 10^5$ nanocrystals of identical size and number of dopants is simulated. After all the nanocrystals are checked $\Phi(n,k)$ is identified as the fraction of all the nanocrystals that contained at least one pair-state (i.e. a valid solution to equation (3)). The algorithm replaces in each nanocrystal a fixed fraction f of the n lattice positions with dopant ions. However, a realistic procedure would be to replace each lattice position with a dopant ion with a probability f because a random distribution of dopants in the nanocrystal is assumed. A random distribution of dopant ions is a realistic assumption if the host lattice and the dopant ions have a very similar size and chemical properties, as is in the case of, for example, rare earth compounds doped with (other) rare earth ions. A random situation will result in a binomial distribution of the number of dopant ions present in the nanocrystal with expectation value k. Using this, combined with the knowledge of $\rho(n)$, the expression for finding at least one pair-state in the nanocrystal is given by

$$\mathcal{P}(\rho, f) = \sum_{i=2}^{n} \left(\begin{array}{c} n \\ i \end{array} \right) f^i (1-f)^{n-i} \Phi(n,i) \ , \tag{4}$$

where the summation begins with $i = 2$, because at least two dopant ions are required to form a pair-state.

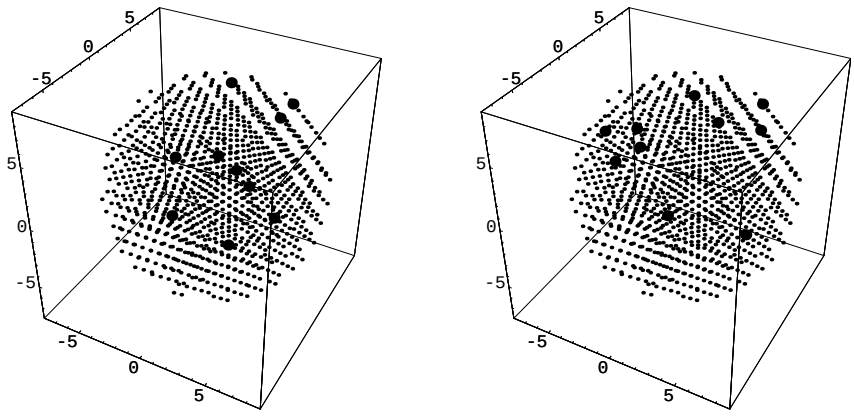

Figure 3: Two typical simulations obtained for $\rho = 4$ and $f = 0.01$. The small dots ($\cdot$) represent the lattice and the large dots ($\bullet$) indicate the dopants present in this lattice. The figure is discussed further in the text.

The percentage of pair-states relative to the total number of dopants present in the nanocrystal is found through a similar algorithm. Again $1 \cdot 10^5$ nanocrystals of identical size and number of dopants are simulated. The total number of valid solutions of equation (3) found in these $1 \cdot 10^5$ nanocrystals is defined as $\Psi(n, k)$. For small f, the percentage of dopants that are part of a pair-state is $2\Psi(n, k)/k \cdot 100\%$. This finally results in

$$\mathcal{Q}(\rho, f) = 2 \sum_{i=2}^{n} \left(\begin{array}{c} n \\ i \end{array} \right) f^i (1-f)^{n-i} \frac{\Psi(n,i)}{nf} \cdot 100 \ \ [\%] \ , \tag{5}$$

through a similar argument as was used for equation (4).

Two typical simulations are shown in figure 3. These examples were calculated using $\rho = 4$ (i.e. $n = 1048$) and $f = 0.01$ (i.e. $k = 10$). In the simulation on the left, a pair-state has formed as can be seen in the top right part of the simulated crystal. The simulation on the right did not result in a pair-state. For this specific case, values were found of $\mathcal{P}(4, 0.01) = 0.3921$ and $\mathcal{Q}(4, 0.01) = 10.80\,\%$.

2.3.2 Probability for at least one pair-state

The results of the calculation of $\mathcal{P}(\rho, f)$ for $1 \leq \rho \leq 8.5$ are shown in figure 4. Note that for large ρ the probability distribution will converge monotonically to a step function. This result is straightforward, since $\mathcal{P}(\rho, f)$ denotes the probability of finding *at least one* pair-state in the crystal.

Upon close inspection of figure 4, it is noted that for small particles the surface contribution to the probability distribution is very large. The fact that lattice posi-

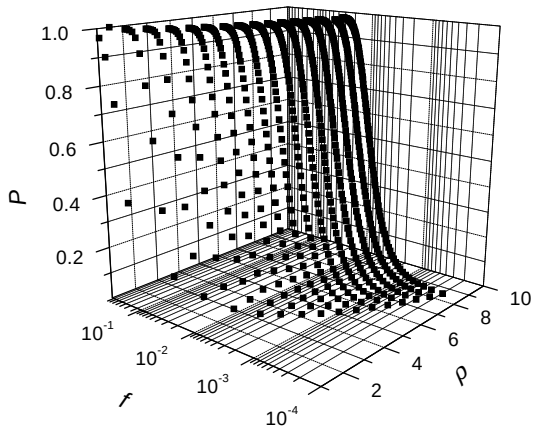

Figure 4: The probability distribution $\mathcal{P}(\rho, f)$, which describes the probability to find at least one pair-state in a zincblende nanocrystal with expanded radius ρ and dopant fraction f. Note the logarithmic scale for the f-axis.

tions on the surface have only 8 neighbours, instead of the usual 12 for bulk lattice positions, results in a drastic increase of the probability for pair-state formation compared to larger crystals. This is seen clearly from the following example: For $\rho = 7$ the surface contribution will be relatively small and the simulation shows $\mathcal{P}(7, 0.0052) = 0.57$. If the surface did not influence the probability distribution, then $\mathcal{P}(2, f) = 0.57$ can be solved easily through $f = (7/2)^3 \cdot 0.0052 = 0.22$ because of the cubic dependence of n on ρ. However, the simulations show that $\mathcal{P}(2, 0.043) = 0.57$. The much smaller (about 5 times) dopant-fraction required (0.043 vs. 0.22) is a direct result of the larger surface contribution to the probability distribution.

2.3.3 Pair-state concentration

In this section the results obtained from the simulations of $\mathcal{Q}(\rho, f)$ in the low-dopant concentration regime are described. It is important to stay roughly in the $0 < f < 0.1$ range, because for larger f the presence of triple-states needs to be taken into account. For these states, defined to occur if and only if

$$\exists \lambda \neq \sigma \neq \mu \neq \lambda \in \mathbb{Z} : |\mathbf{q}_\sigma - \mathbf{q}_\mu| = d_{\mathrm{NN}} = |\mathbf{q}_\lambda - \mathbf{q}_\sigma| \,, \tag{6}$$

the symmetry properties of the problem can no longer be exploited. This is seen by the fact that a triple-state in the zincblende structure can be three particles on a line (which would count as four dopants being part of a pair-state in the algorithm

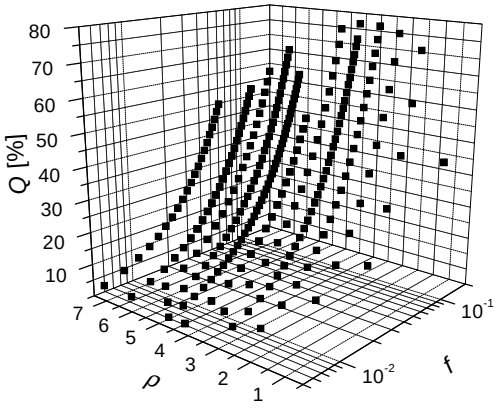

Figure 5: The probability distribution $\mathcal{Q}(\rho, f)$, which describes the expected percentage of pair-states in a zincblende nanocrystal with respect to the total number of dopants present in this nanocrystal. Note the logarithmic scale for the f-axis.

presented in section 2.3.1), or three particles in a triangle shape (counting as six parts of a pair-state). The combinatorial problems associated with these "higher-order" corrections become increasingly more difficult to handle and require much more computer-time to be correctly evaluated. Therefore, the remainder of this analysis will only focus on the low dopant range ($0 < f < 0.1$), and the presence of triple-states will be ignored. With this assumption equation (5) describes the percentage of pair-states in the nanocrystal.

Figure 5 shows $\mathcal{Q}(\rho, f)$ determined by evaluating equation (5) for $1 \leq \rho \leq 7$. The influence of the surface (and thus size) can be seen clearly in the data, just as in the previous section. If the surface did not influence the results, then one would expect $\mathcal{Q}(2, f) = \mathcal{Q}(7, f)$ for all f. However, the data show that $\mathcal{Q}(2, 0.04) = 1.73\%$, while $\mathcal{Q}(7, 0.04) = 0.77\%$. This difference is explained by the increased probability for pair-state formation of a dopant at the surface of the nanocrystal with respect to a bulk dopant (due to the difference in coordination number). All data presented in this figure could be fitted well using a linear relation of $\mathcal{Q}(\rho, f)$ as a function of f, which is also expected. For low-dopant fractions, there are almost no triple-states, and this is the reason that the definition of $\mathcal{Q}(\rho, f)$ has the factor 2 (shown in equation (5)). In other words, for small f, if no triple-state is present in the nanocrystal, then addition of one more dopant pair-state will most likely also not result in a triple-state. This means that the concentration of pair-states increases linearly with the number of dopants.

2.4 General formulation of the problem

This section is devoted to deriving closed-form approximations of $\mathcal{P}(\rho, f)$ and $\mathcal{Q}(\rho, f)$ as well as a measure of the uncertainty in the approximation. The results have general applicability to all types of nanocrystals and therefore require a description of the crystal structure. This can be done by making the results dependent on the number of neighbours of a bulk lattice position (the bulk connectivity, C_b), the number of neighbours of a surface lattice position (the surface connectivity, C_s) and a factor determining the number of lattice positions present in the unit-cell (ψ, defined in equation (7)). However, before $\mathcal{P}(\rho, f)$ and $\mathcal{Q}(\rho, f)$ can be discussed, the fraction of surface sites needs to be known. Therefore, in section 2.4.1 a simple first-order equation will be derived that allows the calculation of the fraction of lattice positions present at the surface of the nanocrystal.

2.4.1 Lattice position configuration

The algorithm presented in section 2.3.1 can be applied to derive the number of "bulk" and "surface" lattice positions, denoted as $n_b(\rho)$ and $n_s(\rho)$ respectively. Here, a lattice position is defined to be a surface position if it contributes to $n(\rho)$ but not to $n(\rho-1)$. The total number of lattice positions, given in equation (2) for the zincblende crystal structure, can be generally defined as

$$n(\rho) \;=\; \sum_{\forall \mathbf{p}} 1 \;\approx\; \frac{4\pi\psi}{3}\rho^3 \;, \tag{7}$$

where ψ is the number of lattice positions in the crystal unit cell. The evaluation of the summation was used in section 2.3.1 and gives an exact value for $n(\rho)$.

When the assumption indicated in the second part of equation (7) is made, then the number of surface lattice positions is given by

$$n_s(\rho) \;=\; n(\rho) - n(\rho-1) \;=\; 4\pi\psi\left[1 + 3\rho(\rho-1)\right]/3 \;, \tag{8}$$

and the number of bulk lattice positions by

$$n_b(\rho) \;=\; n(\rho-1) \;=\; 4\pi\psi\left[\rho-1\right]^3/3 \;. \tag{9}$$

The fraction of lattice positions that is located at the surface of the nanocrystal, $\delta n(\rho)$ can be expressed in terms of $n_s(\rho)$ and $n(\rho)$ and yields

$$\delta n(\rho) \;\equiv\; \frac{n_s(\rho)}{n(\rho)} \;=\; 3\rho^{-1}(1-\rho^{-1}) + \rho^{-3} \;. \tag{10}$$

Note that $\delta n(\rho)$ no longer depends on ψ.

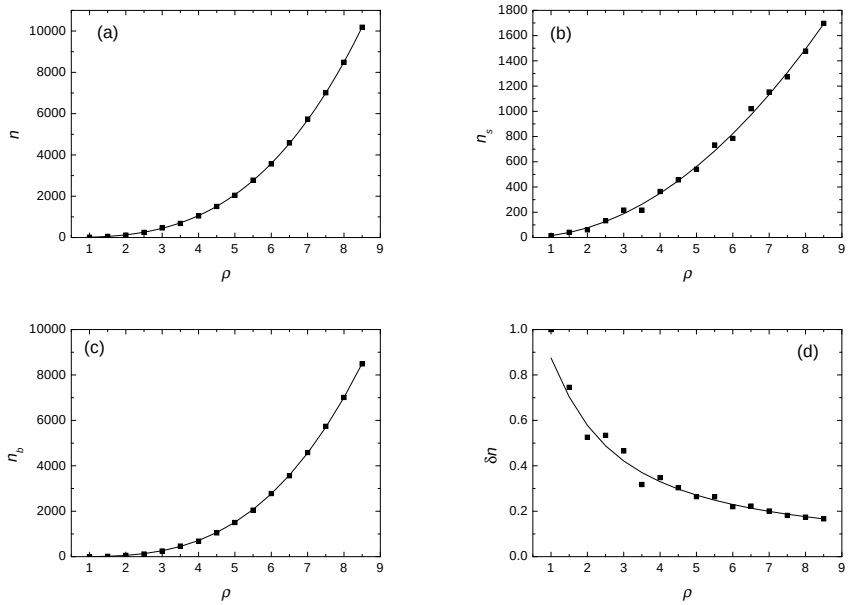

Figure 6: Comparison between the exact summation and the approximation presented in equation (7). The squares in (a) through (d) represent the values found for $n(\rho)$, $n_s(\rho)$, $n_b(\rho)$ and $\delta n(\rho)$ from the simulations presented in section 2.3 (i.e. the evaluation of the sum in equation (7)). The lines through the data are predictions from equations (7) through (10), using $\psi = 4$.

The squares in figure 6(a)$-$(d) show the values that were found for $n(\rho)$, $n_s(\rho)$, $n_b(\rho)$ and $\delta n(\rho)$ respectively. For these values the assumption of equation (7) was not made, but the exact crystal configuration was used by means of the simulation-data presented in section 2.3 (i.e. the complete sum in equation (7) was evaluated). However, as can be seen from this figure, the lines through the data, resulting from equations (7)- (10) indicate a good agreement between this first-order theory and the nanocrystal structure. Note that the line through the data in figure 6 (d) does not depend on ψ and is a direct prediction of the theory described above. This is significant, because it implies that $\delta n(\rho)$ as described in equation (10) is independent of the crystal structure. As is indeed expected, the limit $\rho \to \infty$ for equation (10) is 0. This agrees very well with the data presented in the figure. From the data in figure 6 it may be concluded that equation (2) is a good approximation in the zincblende case, even for a very small nanocrystal (such as $\rho = 2$).

2.4.2 Poisson approximation

In this section, an approach is discussed which enables the computation of approximations of $\mathcal{P}(\rho, f)$ and $\mathcal{Q}(\rho, f)$ for any given crystal, without any simulations. In addition, a rigorous upper bound of the error in the approximation of $\mathcal{P}(\rho, f)$ is presented. The method that will be used is a special case of the Stein-Chen Poisson approximation method [25]. The main idea is that the number of pair-states is close in distribution to a Poisson random variable; this is due to the fact that the pair-states are almost independent. If the pair states were completely independent, then the total number of pair-states would have a binomial distribution. The binomial distribution is, under the conditions relevant to this discussion, very close to a Poisson distribution [26]. The different pair-states in a nanocrystal turn out to be sufficiently independent as to make an approximation with a Poisson distribution extremely useful.

The total number of nearest neighbour pairs in the crystal is denoted by N. This results, in the notation introduced in section 2.4.1, in

$$\begin{aligned} N &= \frac{1}{2}(n_s C_s + n_b C_b) \\ &= \frac{2\pi\psi(\rho-1)}{3}\left[(\rho-1)^2 C_b + (3\rho + (\rho-1)^{-1})C_s\right] . \end{aligned} \tag{11}$$

The probability that a lattice position contains a dopant is denoted by f. Therefore, the expected number of dopant pair-states will simply be given by $Nf^2 \equiv \lambda$.

The number of pair-states in the nanocrystal will have approximately a Poisson distribution with expectation value λ. This implies that the probability of finding x pair-states in the nanocrystal will be approximated by $P(x) \equiv e^{-\lambda}\lambda^x (x!)^{-1}$. Therefore, the probability of finding at least one pair-state in the nanocrystal will be approximately $\mathcal{P} = 1 - P(0) = 1 - e^{-\lambda}$. Because λ represents the (expected) number of dopant pair-states, the percentage of dopants that are part of a pair-state is approximated by $\mathcal{Q} = 2\lambda/k \cdot 100[\%]$. Hence $\mathcal{P}$ is the approximation of $\mathcal{P}(\rho, f)$, and $\mathcal{Q}$ is the approximation of $\mathcal{Q}(\rho, f)$. Now $\mathcal{P}$ and $\mathcal{Q}$ can be written as

$$\mathcal{P} = 1 - \exp\left[-\frac{2\pi\psi f^2}{3}\left\{C_b(\rho-1)^3 + C_s(3\rho(\rho-1)+1)\right\}\right] , \tag{12}$$

and

$$\mathcal{Q} = \frac{[1+3\rho(\rho-1)]C_s + [\rho-1]^3 C_b}{\rho^3} f \cdot 100[\%] . \tag{13}$$

It is interesting to note that equation (12) has indeed a stretched-Boltzmann form and equation (13) is linear in f. These observations agree with the results from the simulations shown previously.

It can be proven that the error introduced by this approximation is bounded by [27]

$$|\mathcal{P}(\rho,f)-\mathcal{P}| \leq \left(1-e^{-Nf^2}\right)\{\frac{4\pi\psi(f+f^2)}{3N}[(\rho-1)^3C_b(C_b-1)+ (1+3\rho(\rho-1))C_s(C_s-1)]+f^2\}\ . \quad (14)$$

The numbers resulting from equations (12), (13) and (14) can be easily computed, and this means that simulations are no longer needed. As long as the upper bound for the error in $\mathcal{P}$, as found from the evaluation of equation (14), remains small, the Stein-Chen Poisson approximations of $\mathcal{P}$ and $\mathcal{Q}$ can be used directly.

As an example, consider the zincblende crystal structure of section 2.3.1, where $\psi = 4$, $C_b = 12$ and $C_s = 8$. The evaluation for $\rho = 4$ and $f = 0.01$ leads to $\mathcal{P} = 0.405$ and $\mathcal{Q} = 10.4\%$. These numbers are in very good agreement with the simulations presented in section 2.3.1. The upper bound of the error is $|\mathcal{P}(\rho,f) - \mathcal{P}| = 0.074$. The simulations of section 2.3 indicate that the actual error (0.013) is even smaller than the theoretical upper bound that was obtained.

It is of interest to decide when the Stein-Chen Poisson approximation works satisfactorily. An estimate of the right hand side of equation (14) shows that the maximum error is small when f is of the order of $1/\sqrt{N}$ or smaller. However, a large maximum error does not necessarily give a large discrepancy between the Poisson approximation and the simulated data. This is caused by the fact that the upper bound as defined in equation (14) is a 'worst-case' scenario. Apparently, the error introduced by the Poisson approximation is much smaller than this worst-case error.

2.5 An example

As a typical example, the probability for the formation of at least one pair, and the average percentage of pair-states in a ZnSe:Mn^{2+} sample with an average nanocrystal radius of 3.4 nm are calculated. The ZnSe lattice has a zincblende structure ($\psi = 4$, $C_b = 12$ and $C_s = 8$) with a lattice parameter $a = 5.6676$ Å (i.e. $r = 3.4$ nm $\Leftrightarrow \rho = 6$) and the Mn^{2+} dopant ions are located on the Zn^{2+} lattice position.

The results from the simulations presented in sections 2.3.2 and 2.3.3 can be used directly. These nanocrystals contain 3564 lattice positions, 785 (22 %) of which are on the surface of the crystal. Table 1 shows both the simulated results and the results obtained in the Poisson approximation. The expectation value for the total number of dopants present in the lattice, k, is also included.

The results from the Poisson approximation are in very good agreement with the simulation data. Even for the larger dopant fractions very small differences

		Simulations		*Poisson theory*	
f	k	$\mathcal{P}(6,f)$	$\mathcal{Q}(6,f)$	$\mathcal{P}$	$\mathcal{Q}$
0.002	8	0.073	1.56 %	0.072	2.06 %
0.004	15	0.277	3.82 %	0.258	4.13 %
0.007	26	0.638	6.96 %	0.599	7.22 %
0.009	33	0.789	9.11 %	0.780	9.28 %
0.012	44	0.943	12.3 %	0.932	12.4 %
0.015	55	0.989	15.4 %	0.985	15.5 %
0.02	73	0.999	20.8 %	0.999	20.6 %
0.05	181	1.000	52.9 %	1.000	51.6 %

Table 1: Results for a ZnSe nanocrystal with a radius of 3.4 nm and a dopant fraction f. Both the results from the simulations (section 2.3) and from the Poisson approximation (section 2.4.2) are shown.

are observed. This result is important because for this ZnSe nanocrystal $N = 39628$, so the error of the approximation is expected to become large for $f > 0.01$. However, as can be seen from the table, the difference between the Poisson approximation and the simulation data remains small, indicating that the Poisson approximation will continue to yield reliable data for higher dopant fractions.

3 Single nanocrystals

The second part of this chapter is devoted to the study of single luminescent nanocrystals. Luminescence spectroscopy of single nanocrystals started roughly six years ago, with techniques that were developed for single molecule spectroscopy. The observation of luminescence from a single nanocrystal eliminates ensemble averaging effects and has provided a wealth of new information on the luminescence properties of nanocrystalline semiconductors. After a discussion of the synthesis of a typical nanocrystal (CdSe nanocrystal covered with a ZnS shell) and a description of the experimental setup, several typical and interesting results will be shown. This part will end with a few challenges for future research (exercises for the interested reader ...).

3.1 Experimental

3.1.1 Chemical synthesis of the nanocrystals

The chemical synthesis of semiconductor nanocrystals can be challenging. The synthesis of the most efficiently luminescing CdSe/ZnS core/shell nanocrystals, which are mostly used in single nanocrystal luminescence experiments, inolves some chemicals that can react strongly with water or oxygen. Therefore, the complete synthesis is performed in a glovebox (a dry nitrogen atmosphere).

The remainder of this section deals with so-called *core/shell* nanocrystals. A second type of semiconductor is (chemically) grown around the original nanocrystal (the core). This shell has a larger bandgap than the core and a comparable lattice parameter and crystallographic structure. The presence of the (larger bandgap) shell confines the electron and hole within the nanocrystal core. The shell also passivates the surface of the nanocrystal, which will result in an increased luminescence efficiency through the removal of non-radiative decay paths such as surface defects. A typical example of a synthesis is ZnS-capped CdSe; nanocrystals can be made using a TOP/TOPO method similar to the one described by Hines and Guyot-Sionnest [28]. Chemicals that are used in this synthesis are Tri-*n*-octylphosphine (TOP), Tri-*n*-octylphosphine oxide (TOPO), anhydrous methanol, anhydrous chloroform, diethylzinc, dimethylcadmium, bis(trimethyl)-silylsulphide ($(TMS)_2$) and selenium powder.

The synthesis is performed in a glovebox filled with nitrogen. Stock solutions of Cd, Zn, S and Se precursors in TOP are first prepared. For the Cd/TOP stock solution 1.6 g dimethylcadmium is dissolved in 15.5 ml TOP. The Zn/TOP stock solution is prepared by dissolution of 1.23 g diethylzinc in 9.0 ml TOP. 1.3 g Se is dissolved in 16.0 ml TOP and 2.0 ml $(TMS)_2S$ is dissolved in 8.0 ml TOP to obtain the Se/TOP and S/TOP stock solutions, respectively. Cd/Se/TOP and Zn/S/TOP stock solutions are always freshly prepared for each synthesis. The Cd/Se/TOP stock solution is prepared by diluting 0.4 ml Cd/TOP and 0.4 ml Se/TOP in 2.0 ml TOP. By dissolving of 1.6 ml S/TOP and 1.12 ml Zn/TOP in 8.28 ml TOP, one obtains the Zn/S/TOP stock solution.

The concentrations of the chemicals are chosen such that the overcoated nanocrystals will have about 7 monolayers of ZnS surrounding the CdSe core. The calculation of the number of monolayers is based on the amounts of precursors used in the synthesis and one $Zn-S$ length is defined as one monolayer.

The synthesis is now performed in the following way. First, 25 g TOPO is heated to 300 °C and kept at this temperature for half an hour to degass and dry the TOPO. The temperature is then raised to 370 °C. Next, the heater is removed and the temperature begins to drop. At 360 °C 1.4 ml Cd/Se/TOP stock solution (containing 0.13 mmol Cd and 0.20 mmol Se) is injected rapidly. The reaction

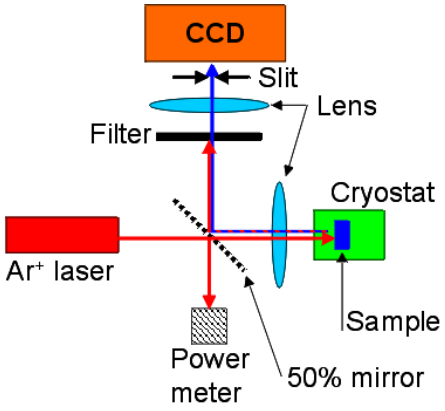

Figure 7: A schematic overview of the setup used to detect the luminescence from a single nanocrystal.

mixture is allowed to cool to 300 °C and at this temperature 13.73 ml of the Zn/S/TOP stock solution (1.55 mmol Zn, 2.20 mmol S) is added in five portions at approximately 20 s intervals. After this injection the reaction mixture is allowed to cool down to 100 °C and is kept at this temperature for one hour. The suspension is purified by precipitation of the nanocrystals with anhydrous methanol. The precipitate is collected by centrifuging (4000 rpm, 5 minutes) and then washed three times with anhydrous methanol. The nanocrystals are finally dispersed in doubly distilled chloroform to give a clear colloidal suspension of nanocrystals in chloroform.

3.1.2 Single nanocrystal luminescence setup

For single particle luminescence measurements, small droplets of a strongly diluted NC stock solution (roughly 10^{-9} mol NC per liter) were deposited, spin-coated ($\sim$2000 rpm) and dried on single crystal quartz slides. The final density was approximately 0.1 NC/μm^2. This very low density makes it possible to optically resolve each dot separately. The slides were prepared, mounted and finally sealed in a cryostat.

Figure 7 shows the far-field[4] epifluorescence setup that can be used to detect the luminescence of a single nanocrystal. The 514.5 nm line of an Ar^+ ion laser is partly transmitted through a mirror onto the nanocrystals (focussed to a spot size of roughly 25×25 μm^2) and the emission is focussed on the entrance slit of a CCD

[4]For a clear and thorough discussion of the differences between far-field and near-field spectroscopy, please look at "*Optical near-field microscopy and spectroscopy: introduction and examples*" by Prof. Wegener. This chapter can be found elsewhere in this book.

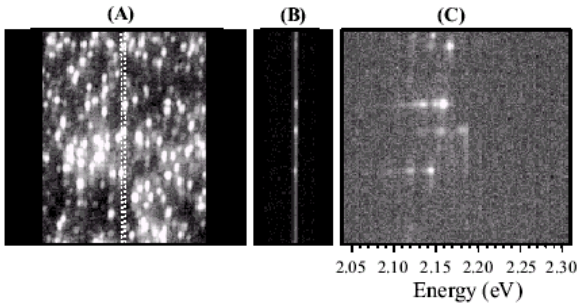

Figure 8: (a) Luminescence of single CdSe nanocrystals (45 Å) recorded at 10 K with the entrance slit fully open. (b) The same, but now with the slits nearly closed. (c) Spectrally resolved analogon of the data shown in (b). Each of the spectra is due to a single nanocrystal. Data taken from Ref. [29] with kind permission from the authors.

setup. This setup contains an entrance slit, a monochromator (in zero order) and a CCD camera (initially in imaging mode). When the slit is fully open, and the CCD is used in imaging mode, an image such as that shown in figure 8(a) is obtained. Each of the dots in this image is the luminescence of a single nanocrystal. In order to measure the emission spectrum of one of the nanocrystals, the entrance-slit is narrowed to e.g. 10 μm, as is shown in figure 8(b).

The grating in the monochromator is now switched from the mirror function (zero order) to a wavelength region of interest. The emission from the single nanocrystals, which is focussed on the narrow slit, is dispersed by the grating and the emission intensity is measured as a function of wavelength (or energy) with the CCD camera in spectroscopy mode. In figure 8(c) the different horizontal traces represent the emission spectra for which the emission is focussed on the entrance slit at different heights (compare to figure 8(b)).

3.2 Luminescence of a single nanocrystal

In the previous section, it was indicated that the emission spectra (e.g. in figure 8(c)) are spectra from single nanocrystals. An obvious question now is how to prove that a spectrum is really due to a *single* nanocrystal. In order to verify this, the temporal evolution of the luminescence intensity and wavelength will now be discussed.

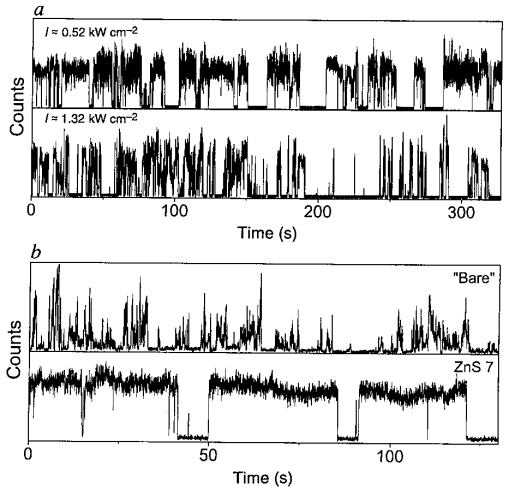

Figure 9: Time dependence of the emission intensity of a single CdSe nanocrystal. Excitation was at 514 nm, and the measurement was performed at 4 K. Data taken from Ref. [30] with kind permission from the authors.

3.2.1 Blinking

When the luminescence intensity at a given wavelength is studied as a function of time (at constant excitation intensity), traces such as those shown in figure 9 are measured. This typical behaviour was first observed in the group of Brus [30]. The time trace shows luminescence fluctuations between'on' and 'off'. After emitting light at a certain count rate, the dot turns 'off' for a period of time and no light (counts) are detected until the dot turns 'on' again. This observation of luminescence intermittancy (the discrete changing from an 'on' to an 'off' state, or "blinking") is a direct proof that the luminescence originates from a single nanocrystal. If the luminescence of two (or more) nanocrystals was being detected, a different variation of the intensity would be expected. After all, it is very unlikely that both (or all) dots would turn 'off' and 'on' at exactly the same moment.

It is interesting to observe in figure 9(a) that on increasing the excitation density (in this case from 0.52 kW/cm^2 to 1.32 kW/cm^2) a clear increase in the blinking rate is observed. Also, for higher laser powers more time is spent in the 'off' state. Figure 9(b) shows the effect of the ZnS coating layer on the blinking characteristics. It is immediately clear from this comparison that a core/shell system is much less prone to blinking than a bare nanocrystal. At the end of the next section an explanation of these results will be presented and discussed.

Figure 10: Correlation between blinking of a CdSe/ZnS nanocrystal (measured at 10 K and using $\lambda_{\mathrm{ex}} = 514$ nm) and a shift in the average emission wavelength. Data taken from Ref. [32] with kind permission from the authors.

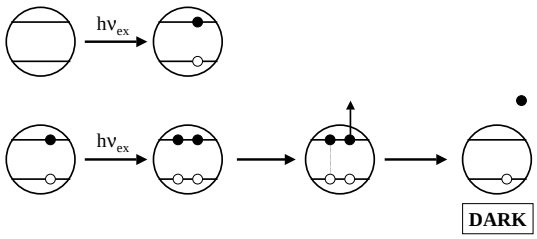

Figure 11: Schematic explanation of the blinking and shifting of the luminescence of a single nanocrystal. Explained in detail in the text.

3.2.2 Recoverable changes

In addition to the time evolution of the intensity, a change of the emission spectra with time has also been observed for single nanocrystals. In the early publications on single nanocrystal luminescence, discrete changes in the emission were observed. In addition to random spectral shifts, a continuous blue shift of the emission spectra was also observed (discussed in detail in section 3.2.3). Again, the discrete changes in the emission spectra provide evidence that the emission results from a single nanocrystal.

In a recent publicaton by the group of Bawendi an interesting relation was established between the occurrence of discrete spectral jumps of several meV and the fluorescence intermittance: the emission spectrum was often observed to shift to a different wavelength after a dark period. In figure 10 a typical time trace showing this effect is depicted. The relation between the blinking, described in section 3.2.1 and the shifting, described in this section, can be explained using a simple qualitative model. This model is schematically shown in figure 11.

The upper part of figure 11 shows the absorption of a photon (energy $h\nu_{\mathrm{ex}}$) by the nanocrystal and the subsequent formation of an electron-hole pair. If the electron and hole recombine, the nanocrystal can luminesce (not shown). However, the nanocrystal may also be excited further (lower part of figure 11). When this happenes, a second electron-hole pair is formed inside the nanocrystal. A nanocrystal with two excitons located close together will quickly Auger-quench. In the Auger-quenching process, one electron-hole pair recombines and donates its energy (instead of luminescing) to the electron[5]. The electron will then be either excited into a high vibronic state (from which it will thermalize back to the bottom of the conduction band), or it will be ejected from the nanocrystal core and transferred to a localized state near the surface of the nanocrystal (shown in the lower right part of figure 11). When the first process takes place, the final state will be a nanocrystal with one electron-hole pair in the core. This state can luminesce at the normal nanocrystal wavelength. However, when the second process takes place, the final state will be a nanocrystal with a localized electron in a state near the surface and a delocalized hole trapped in the nanocrystal core. This state is "dark": it cannot luminesce because excitation of the nanocrystal in this state leads to very fast (non-radiative) energy transfer from the exciton to the delocalized hole through the Auger mechanism.

The transition from the dark state back to a "bright" state can occur through three different processes:

1. A charge localized in the vicinity of the nanocrystal relaxes back into the nanocrystal core and recombines with the delocalized hole.

2. The electron that was just ejected from the nanocrystal core through the Auger quenching process relaxes back into the core and subsequentely recombines with the delocalized hole.

3. Further excitation of the nanocrystal results in the presence of a new exciton in the nanocrystal. If this exciton Auger-quenches and ejects the remaining hole from the nanocrystal, then a bright state will arise as well. This process is unlikely, because the Auger-quenching coefficient for electrons is typically larger than for holes. This process (which would reduce the dark-time for increasing excitation densities) has never been observed experimentally.

Note the difference between processes 1 and 2: it really matters *which* localized charge carrier relaxes into the core of the nanocrystal! Through processes

[5]In literature it is generally believed that the Auger quenching in a nanocrystal involves the electron. However, this has not been proven yet. The same processes described here for an electron, could equally apply to a hole. In view of the clarity of this text, no mention of this alternative route will be made.

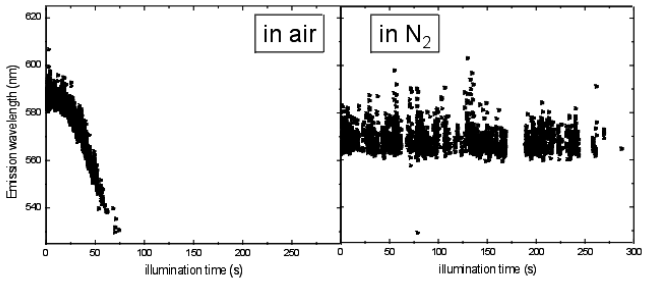

Figure 12: The blue-shifting and bleaching of a CdSe/ZnS nanocrystal. These changes are not reversible. The measurements were performed at room temperature and in air (left) and nitrogen (right) atmospheres under 20 kW/cm^2 of 468 nm excitation. Data taken from Ref. [31] with kind permission from the authors.

1 and 3 the surface dipole and net local electric field will be altered (or generated, if not previously present yet). It is well known that an applied electric field will lead to a shift in emission wavelength of the nanocrystal caused by the Stark effect. Therefore, changing the local electric field (by means of processes 1 or 3) will result in a shift in the maximum emission wavelength. This explains the observed correlation between blinking and spectral shifts in single nanocrystal luminescence.

3.2.3 Irreversible changes

Besides the small shifts that sometimes occur together with the blinking of a nanocrystal, as shown in figure 10, larger and non-reversible changes also take place. These measurements, performed in the group of Gerritsen [31], can be seen in figure 12.

Figure 12 shows the luminescence of single CdSe/ZnS nanocrystals as a function of time at room temperature in two different atmospheres. The measurement on the left was performed in ambient air, while that on the right was performed in a dry nitrogen atmosphere. The average emission wavelengths at $t = 0$ are not the same; this is due to a difference in NC size.

The clear blue-shift of the emission of the CdSe/ZnS nanocrystal measured in air is not observed in a nitrogen atmosphere. The bleaching of the luminescence is also different in nitrogen or air: in air no emission is detected after typically 1 minute, whereas in a nitrogen atmosphere bleaching occurs after about 5 minutes of illumination. When reasonable assumptions regarding the collection efficiency and the solid angle of the detector are made, an estimate can be made

of the total number of photons emitted by a single nanocrystal. In the case of a CdSe/ZnS nanocrystal in air, this resulted in $\sim 10^8$ photons emitted. Note that this is roughly 50 times more than the number of photons emitted from the best single dye molecules. The higher stability of nanocrystals is one of the reasons to use nanocrystals instead of dye molecules as luminescent labels (see also section 3.3.1).

During illumination, the CdSe core is slowly photo-oxidized. As a result of the shrinkage of the CdSe core a blue shift of the emission due to quantum size effects is expected. Furthermore, the formation of surface quenching states causes a gradual decrease of the light output as the emission shifts to shorter wavelengths. Finally, the luminescence disappears and the dot has bleached. Photo-oxidation can explain the shorter bleaching times observed for nanocrystals in air. In a nitrogen atmosphere photobleaching also occurs, albeit after longer illumination times. In view of the high laser power (20 kW/cm^2) photobleaching is not unexpected. Few materials are stable against photodegradation under the laser power used.

3.2.4 Linewidth of the exciton emission

Electron-hole recombination results in exciton emission from a nanocrystal at an energy that corresponds to the bandgap. Emission spectra of an ensemble of nanocrystals usually show rather broad emission lines, even at low temperatures, where a sharp and narrow exciton emission line would be expected. The reason for this is inhomogeneous broadening: due to a variation in particle size, the bandgap varies within an ensemble and each nanocrystal emits at a slightly different energy. Even with the best synthesis techniques, the polydispersity will not be much smaller than 5%, resulting in broad emission lines (especially for smaller nanocrystals where the bandgap varies more strongly as a function of size) [34]. With the possibility of measuring emission spectra of single nanocrystals, the problem of inhomogeneous broadening is solved and indeed narrow emission lines are measured at low temperatures. From a fundamental point of view it is interesting to measure the homogeneous linewidth of the exciton emission at low temperatures, where there is no line broadening as a result of lifetime broadening due to fast phonon induced dephasing processes.

Figure 13(a)-(c) shows three measurements of the linewidth of the same CdSe/ZnS nanocrystal, from which values of 4.6, 2.4 and 0.94 meV have been extracted for the exciton linewidth. This large difference is related to the different excitation densities used: for higher excitation densities (314 W/cm^2) there is considerably more line broadening, in comparison to lower excitation densities (e.g. 65 W/cm^2).

A more systematic study of the measured linewidth as a function of excitation density (either laser power, or integration time) is presented in figures 13(d),(e). These figures show that increasing excitation densities leads to increased linewidths.

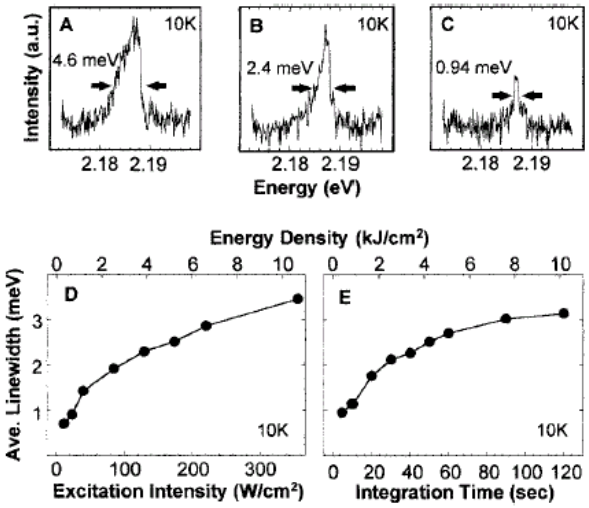

Figure 13: (a)-(c) Several representative measurements of the linewidth of a single nanocrystal. Measured at 10 K using excitation densities of 314, 150 and 65 W/cm^2 respectively. (d),(e) Influence of the excitation density and integration time on the linewidth observed. Data taken from Refs. [29] and [35] with kind permission from the authors.

The explanation for this change in the linewith is related to the spectral shift that was shown in figure 10. As discussed above, light induced photo-ionization of nanocrystals results in a reorganization of the charge distribution around the nanocrystal. The change in electric field influences the resonance frequency (through the Stark effect) and thus the emission wavelength of the single nanocrystal emission spectrum changes during illumination. The higher the laser power, the more frequent is photo-ionization. Increased spectral wandering at higher laser powers results in power broadening as observed in figure 13(d). If the measuring time is increased, there will also be more spectral shifts related to ionization events within the measurement time and a larger linewith is measured (as is observed in figure 13(e)). So, even though one would expect to measure a homogeneous linewidth for a single nanocrystal, there is still inhomogenous broadening, not because there is emission from different nanocrystals with a different local environment, but because the local environment of a single nanocrystal changes in time.

In order to measure the homogeneous linewidth of a single nanocrystal, it is important to use low excitation powers, short measurement times and stable core/shell nanocrystals. The narrowest linewidth in a chemically synthesized nanocrystal has been reported by the group of Bawendi for a 4.3 nm CdSe/ZnS

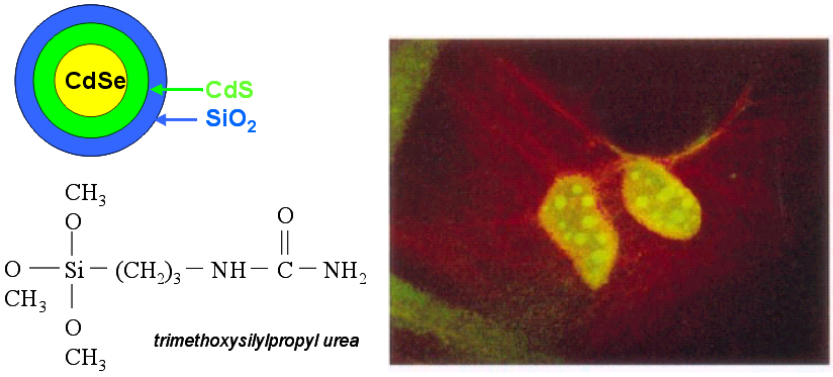

Figure 14: (Left) Schematic representation of the nanocrystal and the structural formula of the coupling agent used. (Right) Measurement from Ref. [36] (with kind permission from the authors) that shows the transport of nanocrystals into the nucleus of a mouse cell.

nanocrystal. The integration time was 6 seconds and the excitation intensity was 25 W/cm^2. The linewidth of 120 μeV (equivalent to an energy of roughly 1 cm^{-1}) was equal to the spectral resolution of the monochromator, showing that the homogeneous linewidth is at most 1 cm^{-1}.

3.3 Applications and challenges for the future

As was already mentioned in section 3.2.3, nanocrystals are a very promising class of materials, especially for labelling applications. This section will describe only one example of biological labelling using nanocrystals, but the interested reader should have no problem finding many more examples in recent literature (such as *Science* or *Nature*). Finally, this section ends with two selected challenges for future research.

3.3.1 Biological labeling using nanocrystals

Nanocrystals have the potential of overcoming the problems encountered with organic dyes by combining the advantages of readily tunable spectral properties, a high photobleaching resistance and a good chemical stability. Due to the broad excitation band, combined with the very narrow emission band, color images can be obtained in which different sizes of nanocrystals are coupled to different molecules or proteins. In the example by the group of Alivisatos that will be discussed next, the color image shows the accumulation of the nanocrystals in specific parts of the cell.

Figure 14 shows a schematic representation of the 'core/shell/shell' structure used in these experiments. The CdSe core and CdS shell are synthesized using methods similar to those discussed in section 3.1.1. The additional SiO_2 shell does not fully cover the core/shell particle, but consists of several silica islands on the CdS shell. When such a nanocrystal is dissolved in a solution containing trimethoxysilylpropyl urea (see figure 14 for the structural formula) then the silica will bind to the silyl-group, thus forming a "ball on a chain".

The solution with the nanocrystals is now brought into contact with the surface of a cell. Because the long molecule attached to the nanocrystal has a urea group ($NH-CO-NH_2$) at the end, the complete system is transferred into the nucleus of the cell due to the gradient in the chemical potential. Loosely speaking, this can be thought of as 'nature takes care of this for you'. Note that this only works if the bond between the urea and the NC is rather strong and the nanocrystal is not too large. When a luminescence image is now recorded, data such as shown on the right of figure 14 are obtained. The complete picture shows two cells of a mouse (3T3 mouse fibroblast cells). The two grayish blobs near the center are the nuclei of the cells. The bright spots in the nuclei are due to the luminescence of nanocrystals which has been transported through the cell membrane into the nucleus.

The initial labelling experiments discussed here show the great potential of nanocrystals in this field. The main advantages (in comparison with dye molecules) are the high stability, the broad excitation range and the narrow emission spectrum. However, there are also disadvantages: the nanocrystals are relatively large and the blinking behavior is a problem in certain types of experiments. The linking of nanocrystals to biological molecules is still a challenge which is being addressed in various research groups.

3.3.2 Membrane signal transduction

Another area in which the high stability, tunability and favourable spectral properties (broad excitation, narrow emission) of nanocrystals may be advantageous is in real-time studies of signal transduction through a cell membrane. The first step in such a process is often the coupling of a protein in the cell to a membrane protein. To study the coupling (and decoupling) of the proteins one can use resonant energy transfer between different dye molecules or between nanocrystals and dye molecules. The idea is shown schematically in figure 15.

The protein in the cell is linked to a nanocrystal and a dye molecule is attached to the membrane protein. Using a confocal microscope, the luminescence can be measured with a high spatial resolution. Excitation occurs at a wavelength which can excite the nanocrystal, but not the dye molecule. Emission from a single nanocrystal can be easily measured in this type of setup. When the two proteins

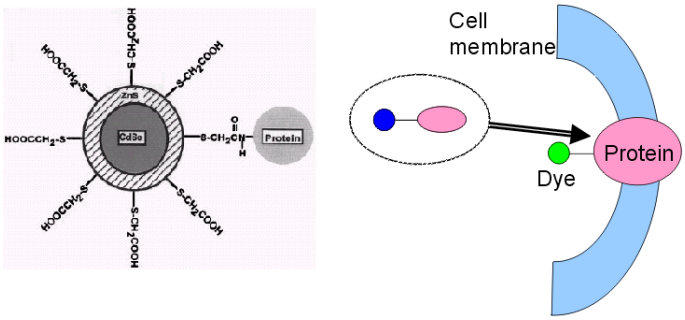

Figure 15: Schematic explanation of the experiment that could be used to measure real-time signal transduction through a cell membrane via a protein. Explained in detail in the text.

couple, the nanocrystal will be positioned close to the dye molecule. If the distance between the dot and dye is small enough (typically less than about 5 nm) in the coupled configuration, energy transfer from the excited nanocrystal to the dye molecule occurs and emission from the dye molecule is measured, while the nanocrystal emission is quenched. By measuring the luminescence spectra as a function of time in the area around a membrane protein the kinetics of coupling and decoupling of the proteins can be followed: as long as nanocrystal luminescence is measured there is no coupling and when dye luminescence is detected, the two proteins are coupled. The time resolution that can be obtained can be as fast as 5 ms per spectrum, allowing for kinetic studies with this time resolution. By attaching a different dye and different nanocrystal to the protein on the outside of the cell membrane, the next step in the signal transduction (coupling of a protein on the outside of the membrane with the other side of the membrane protein) can be followed in real-time as well. These experiments have not yet been performed and the practical realization is one of the challenges in the field.

3.3.3 Excitation spectrum of a single nanocrystal

The understanding of the luminescence mechanism of nanocrystals has greatly benefited from the studies on single nanocrystal luminescence. Further fundamental research aiming at, for example, a better insight into processes responsible for the blinking, the influence of the shape of the nanocrystals, coupling with lattice vibrations, luminescence lifetime studies, polarization dependence and many other topics are being addressed and should result in many interesting papers in the future. One of the greatest challenges in this field is to try and measure an excitation spectrum of a single nanocrystal. In all single nanocrystal luminescence measurements only the emission spectrum for a single dot is measured under ex-

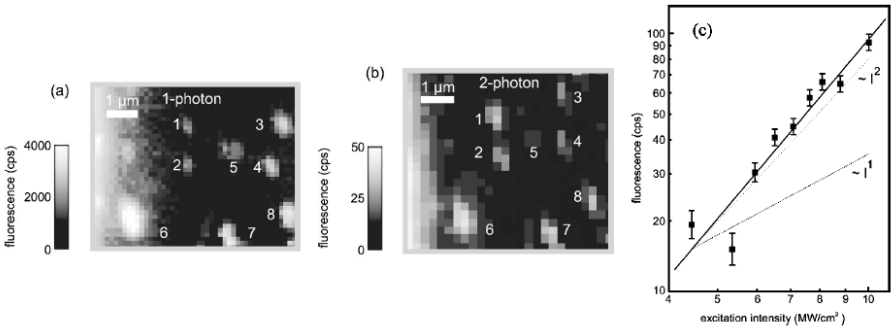

Figure 16: (a) One- and (b) two-photon images of single CdS nanocrystals. Excitation was at 405 nm (one-photon excitation) with an excitation density of 1 kW/cm^2 or at 810 nm (two-photon excitation) with an excitation density of 6 MW/cm^2. The measurement was performed at 4 K. (c) Dependence of the luminescence intensity on the excitation intensity for the two photon experiment. Data taken from Ref. [37] with kind permission from the authors.

citation at a shorter wavelength. The emission spectrum corresponds to the exciton recombination and provides information on the energy difference between the lowest conduction band state and the highest valence band state. Due to quantum size effects this energy difference increases as the particle size is reduced. The relation between particle size and this energy is rather well explained by theoretical models [2]. However, discrete energy levels are also located at higher energies. In the excitation and absorption spectra of an ensemble of semiconductor nanocrystals structure is observed indicating the presence of these discrete energy levels, but inhomogeneous broadening as a result of the particle size distribution hampers the observation of these levels. If an excitation spectrum of a single nanocrystal could be measured, its energy level structure could be determined with high accuracy and it would be possible to compare the measured energy level structure with energy level calculations for an electron-hole pair in a confined structure.

Up until now it has not been possible to measure a single nanocrystal excitation spectrum. The reason is that it is not possible to measure an excitation spectrum while monitoring the exciton emission. The exciton emission is resonant with the lowest energy excitation transition and also close in energy to the higher energy excitation lines which one wants to observe in the excitation spectrum. There are no optical filters for which the cut-off edge is sharp enough to prevent scattered excitation light from reaching the detector. One method to circumvent this problem is using two-photon excitation. By exciting at twice the wavelength and detecting emission at the normal wavelength, filtering is possi-

ble. Using a tunable laser for excitation in the wavelength region corresponding to twice the wavelength (half the energy) of the single photon excitation region of interest, a two-photon excitation spectrum can be measured. The single nanocrystal two-photon excitation spectrum will reveal all excitation transitions of interest. However, it is not easy to measure a two-photon excitation spectrum for a single nanocrystal. The results of initial experiments from the group of Schmidt [37] are shown in figure 16. The luminescence image of a sample of CdS nanocrystals is shown under one-photon (405 nm) and two-photon (810 nm) excitation. The bright spots in the image correspond to single luminescing CdS nanocrystals. The nanocrystals are observed at the same positions in one- and two-photon excitation. Because the transition probabilities for two-photon excitation are so much smaller, a much higher excitation density is used for the two-photon experiment (6 MW/cm^2) in comparison to the one-photon excitation experiment (1 kW/cm^2). Figure 16(c) shows the expected quadratic laser power dependence of the luminescence intensity for the two-photon excitation experiment. To measure two-photon excitation spectra the wavelength of the laser needs to be scanned while monitoring the exciton emission. In principle this is possible but the successful completion of this experiment will involve a struggle for photons . . .

4 Conclusions

In this chapter two very different topics within the broad field of nanocrystal science are discussed. The first part deals with the statistical properties of dopants which are randomly distributed in the nanocrystal lattice. Before simulations were presented, a brief overview of the influence of dopant pair-formation in a bulk crystal were discussed. The simulations could be explained by using Stein-Chen Poisson theory, enabling the calculation of these statistical properties with great accuracy, for different dopant concentrations, lattice structures and crystal sizes.

The second part deals with the luminescence of single nanocrystals. After a discussion of the chemical synthesis of single nanocrystals in a core/shell geometry, the experimental method for measuring single nanocrystal luminescence is described. Several key experiments are presented and especially the blinking and shifting of the luminescence of a single nanocrystal are discussed in detail. Irreversible changes (blue-shift and bleaching) are described and explained. Measurements of the linewidth of a single nanocrystal and attempts at measuring the excitation spectrum of a single nanocrystal are also shown. This part ended with a few pointers towards biological applications and challenges for future research in this exciting field.

Acknowledgements

Part of this work is done in the Research Program of the Priority Program for new Materials (PPM) and was made possible by financial support from the Dutch association for scientific research (NWO). The author acknowledges stimulating discussion with Ronald Meester, Ageeth Bol, Sander Wuister, Paul Peijzel, Wilfried van Sark, Dave van der Heuvel and Marieke van Veen.

Special thanks are due to Andries Meijerink and John Kelly for careful reading of this manuscript and suggesting many improvements.

References

[1] R. Rosetti, R. Hull, J. M. Gibson, and L. E. Brus, *J. Chem. Phys.* **82**, 552 (1985).

[2] L. Brus, *J. Phys. Chem.* **80**, 4403 (1984).

[3] A. Henglein, *Chem. Rev.* **89**, 1861 (1989).

[4] Y. Wang, and N. Herron, *J. Phys. Chem.* **95**, 525 (1991).

[5] B. O. Dabbousi, M. G. Bawendi, O. Onitsuka, and M. F. Rubner, *Appl. Phys. Lett.* **66**, 1316 (1995).

[6] N. C. Greenham, X. Peng, and A. P. Alivisatos, *Phys. Rev. B* **54**, 17628 (1996).

[7] R. Bhargava, *J. Lumin.* **70**, 85 1996.

[8] J. F. Suyver, S. F. Wuister, J. J. Kelly and A. Meijerink. *Phys. Chem. Chem. Phys.* **2**, 5445 (2000).

[9] D. G. Thomas, J. J. Hopfield, and C. J. Frosch, *Phys. Rev. Lett.* **15**, 857 (1965).

[10] J. I. Pankove, *Optical Processes in Semiconductors* (Dover Publications, New York, 1971), p. 61.

[11] C. R. Ronda, and T. Amrein, *J. Lumin.* **69**, 245 (1996).

[12] J. Ferguson, H. J. Guggenheim, and Y. Tanabe, *J. Phys. Soc. Jpn.* **21**, 692 (1966).

[13] B. C. Barthou, J. Benoit, P. Bennalloul, and A. Morell, *J. Electrochem. Soc.* **141**, 524 (1994).

[14] A. L. N. Stevels, and A. T. Vink, *J. Lumin.* **8**, 443 (1974).

[15] K. Riwotzki, and M. Haase, *J. Phys. Chem. B* **102**, 10129 (1998).

[16] H. Eilers, and B. M. Tissue, *Chem. Phys. Lett.* **251**, 74 (1996).

[17] H. S. Yang, K. S. Hong, S. P. Feofilov, B. M. Tissue, R. S. Meltzer, and W. M. Dennis, *J. Lumin.* **83-84**, 139 (1999).

[18] G. Blasse, and B. C. Grabmaier, *Luminescent Materials* (Springer-Verlag, Berlin, 1994).

[19] B. Henderson and G. F. Imbusch, *Optical Spectroscopy of Inorganic Solids* (Clarendon Press, Oxford, 1989), Chapter 10.

[20] M. Oomen, Adv. Mater. **3**, 403 (1991).

[21] S. Shionoya and W. M. Yen, *Phosphor Handbook* (CRC Press, New York, 1998), Chapter 3.

[22] R. E. Behringer, *J. Chem. Phys.* **29**, 537 (1958).

[23] B. Antic, M. Mitric, D. Rodic, Y. Zhong, Y. Artemov, S. Bogdanovich and J. R. Friedman, *Phys. Rev. B* **58**, 3212 (1998).

[24] J. M. Ziman, *Principles of the Theory of Solids* (Cambridge University Press, New York, 1972), Chapter 1.

[25] A. D. Barbour, L. Holst, and S. Janson, *Poisson Approximation* (Clarendon Press, Oxford, 1992).

[26] S. Ross, *A first course in probability* (Collier Macmillan, New York, 1976).

[27] J. F. Suyver, R. Meester, J. J. Kelly and A. Meijerink, *Submitted to Phys. Rev. B* (June 2001).

[28] M. A. Hines and P. Guyot-Sionnest, *J. Phys. Chem.* **100**, 468 (1996).

[29] S. A. Empedocles, R. Neuhauser, K. Shimizu and M. G. Bawendi, *Adv. Mater.* **11**, 1243 (1999).

[30] M. Nirmal, B. O. Dabbousi, M. G. Bawendi, J. J. Macklin, J. K. Trautman, T. D. Harris and L. E. Brus, *Nature* **383**, 802 (1996).

[31] W. G. J. H. M. van Sark, P. L. T. M. Frederix, D. J. van den Heuvel, H. C. Gerritsen, A. A. Bol, J. N. J. van Lingen, C. de Mello Donegá and A. Meijerink, *J. Phys. Chem. B* **105**, 8281 (2001).

[32] R. G. Neuhauser, K. T. Shimizu, W. K. Woo, S. A. Empedocles and M. G. Bawendi, *Phys. Rev. Lett.* **85**, 3301 (2000).

[33] A. Henglein, *Top. Cur. Chem.* **143**, 113 (1988).

[34] S. V. Gaponenko, *Optical Properties of Semiconductor Nanocrystals* (Cambridge University Press, Cambridge, 1998).

[35] S. A. Empedocles, M. Nirmal and M. G. Bawendi, *Phys. Rev. Lett.* **77**, 3873 (1996).

[36] M. Bruchez, M. Moronne, P. Gin, S. Weiss and A. P. Alivisatos, *Science* **281**, 2013 (1998).

[37] A. M. van Oijen, R. Verbeek, Y. Durand, J. Schmidt, J. N. J. van Lingen, A. A. Bol and A. Meijerink, *Appl. Phys. Lett.* **79**, 830 (2001).